Design and Development of a Novel Passive Wireless Ultrasensitive RF Temperature Transducer for Remote Sensing

Trang T. Thai, Jatlaoui M. Mehdi, Franck Chebila, Hervé Aubert, *Senior Member, IEEE*, Patrick Pons, Gerald R. DeJean, Manos M. Tentzeris, *Fellow, IEEE*, and Robert Plana

***Abstract*— A wireless, passive, and ultrasensitive temperature transducer is presented in this paper. The transducer consists of split ring resonators loaded with micro-bimorph cantilevers, which can potentially operate up to millimeter-wave frequencies (above 30 GHz). As the temperature changes, the bimorph cantilevers deflect and result in a shift of the resonant frequency of the split rings. A design is proposed, that has a maximum sensitivity of 2.62 GHz/μm, in terms of frequency shift per deflection unit, corresponding to a sensitivity of 498 MHz/°C for an operating frequency around 30 GHz, i.e. a frequency shift of 1.6% per °C. Theoretically, it's about two orders of magnitude higher than the existing sensors observed in the same class. This sensor design also offers a high Q factor and is ultra-compact, enabling easy fabrication and integration in micro-electromechanical systems technology. Depending on the choice of materials, the proposed designs can also be utilized in harsh environments. As a proof of concept, a prototype is implemented around 4.7 GHz which exhibits a frequency shift of 0.05%/°C, i.e. 17 times more sensitive than the existing sensors.**

***Index Terms*— Micro-electromechanical systems (MEMS) cantilevers, passive remote sensing, radar cross section (RCS), radio frequency transducer, split ring resonators (SRRs), temperature sensor, wireless sensor.**

I. Introduction

PASSIVE sensors are critical and highly desirable in remote sensing platforms, where long term environment controlling and monitoring can take place. In addition, temperature sensing is critical for use in automotive, medical, and industrial applications. More specific applications include monitoring systems for engine operations, space shuttles, aircraft in-flight conditions, and road and bridge maintenance. Therefore, it is highly desirable for the sensors to be wireless, battery-less, compact, and easily integrated with other wireless passive sensors because multi-physical sensing is required for complete environmental monitoring. A wireless, passive temperature transducer is a device without internal power placed at the monitored site that can transform the local temperature into an output signal that can be read wirelessly by a control system located remotely from the monitored site. Some techniques for temperature measurements include those based on thermoelectricity, temperature dependent variation of the resistance of electrical conductors, fluorescence, and spectral characteristics [1]. However, most existing temperature sensors require a power source, and those with high sensitivity suffer from performance degradation above 130 °C [2]–[4]. Recently, a new class of passive, wireless sensors was introduced based on the correspondence between the physical parameters and shifts in resonant frequencies of a resonating structure [5]–[7]. A capacitively-loaded MEMS (micro-electromechanical systems) slot element for wireless temperature sensing of up to 300 °C was introduced [5] but had a low sensitivity of about 580 kHz/°C around 19.4 GHz, i.e. 0.003% of frequency shift per °C.

A new wireless, passive, and ultrasensitive temperature transducer operating at radio frequencies (RF) is proposed in this paper. The transducer consists of split ring resonators (SRRs) integrated with bi-layer micro-cantilevers. The bimorph cantilevers consist of layers of different thermal expansion coefficients that cause them to bend as temperature changes [6]. Utilizing MEMS allows devices to have low costs, small form factors, and ease of fabrication and integration. The SRRs can potentially operate up to millimeter-wave frequencies above 30 GHz. The micro-cantilevers are placed over split gaps of the SRRs. As the cantilevers deflect in response to temperature changes, the resonant frequencies of the SRR are shifted. The bimorph material choices can be varied and adapted for various temperature ranges desired for different applications while requiring little design modification; thus, it may allow sensing applications up to 300 °C or higher. Without loss of generality, a prototype scaled up in size with operating frequency of 4.7 GHz is presented in this paper to demonstrate the proof-of-concept. In a sensing system, sensor nodes should not only provide information about the physical conditions of the surrounding environment, but also allow their unique identifications

Manuscript received January 4, 2012; revised April 6, 2012; accepted May 3, 2012. Date of publication May 30, 2012; date of current version July 24, 2012. The associate editor coordinating the review of this paper and approving it for publication was Prof. Istvan Barsony.

T. T. Thai is with the Georgia Institute of Technology, Atlanta, GA 30318 USA, with CNRS-LAAS, Toulouse 31077, France, and also with Microsoft Research, Redmond, WA 98052-6399 USA (e-mail: trang.thai@gatech.edu).

J. M. Mehdi is with AS+/IPDiA, CNRS-LAAS, Toulouse 31077, France (e-mail: med.mehdi@gmail.com).

F. Chebila is with CNRS-LAAS, Toulouse 31077, France (e-mail: fchebila@laas.fr).

H. Aubert, P. Pons, and R. Plana are with the University of Toulouse, UPS, INSA, INP, ISAE, LAAS, Toulouse 31077, France (e-mail: herve.aubert@enseeiht.fr; ppons@laas.fr; plana@laas.fr).

G. R. DeJean is with Microsoft Research, Redmond, WA 98052-6399 USA (e-mail: dejean@microsoft.com).

M. M. Tentzeris is with the Georgia Institute of Technology, Atlanta, GA 30318 USA (e-mail: etentze@ece.gatech.edu).

Color versions of one or more of the figures in this paper are available online at http://ieeexplore.ieee.org.

Digital Object Identifier 10.1109/JSEN.2012.2201463

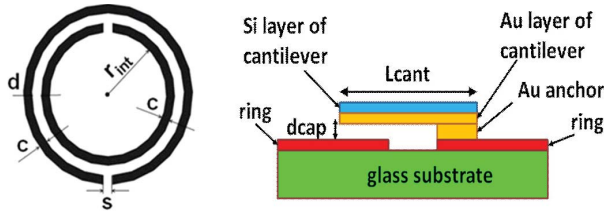

Fig. 1. Topology of the SRRs and bimorph cantilevers.

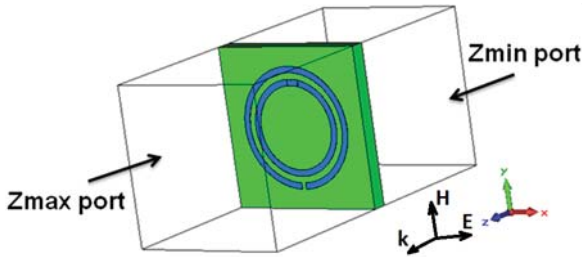

Fig. 2. Setup of the first approach to excite the SRRs.

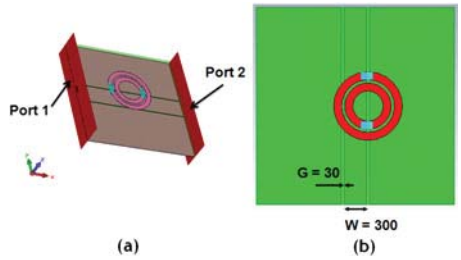

Fig. 3. Setup of the second approach to excite the SRRs with (a) 3-D view and (b) top view of the circuit with substrate not shown and dimensions indicated in micrometers.

in practical networks of multiple sensor nodes. Therefore, based on the approach recently reported in [8] and [9], the authors also propose a newly improved micro-sensor identification technique that allows for an efficient communication between a network of many passive sensor nodes and a central monitoring station. The communication is based on the reading/monitoring of the radar cross section (RCS) level of loaded multi-band scatterers by a frequency-modulated-continuous-wave (FMCW) radar. The RCS measurements of the temperature prototype are performed to illustrate a possible implementation of the transducer in passive, wireless sensing nodes for remote sensing networks. The concept presented in this paper was first introduced in our previous publication [10]. In this extended work, the millimeter-wave designs have been optimized to achieve higher sensitivities, which is included in Sect. II. Additionally, the operational principles of the transducer with an equivalent circuit model are discussed in Sect. III. Direct temperature measurements of the low frequency, proof-of-concept prototype are shown in Sect. IV to address the linear response limits of the sensor. An example implementation of the transducer based on radar cross section measurements is presented in Sect. V, followed by the conclusions in Sect. VI.

II. Designs and Simulations

A. Designs

The transducer consists of double split rings positioned on a dielectric substrate. The slits of the rings are covered with bimorph micro-cantilevers whose layers are made from two different materials, gold with thermal coefficient of 14.1 (10^{-6} K^{-1}) and silicon with thermal coefficient between 4.7 – 7.6 (10^{-6} K^{-1}) [11]. The design of the SRRs integrated with cantilevers is shown in Fig. 1. The dimensions of the split rings are as follows: $r_{int} = 230$ μm, $c = 120$ μm, $d = 50$ μm, and $s = 45$ μm. The substrate is made of glass with dielectric constant $\varepsilon_r = 4.82$ and a thickness of 150 μm. The cantilevers have a length, *Lcant*, of 180 μm, the anchors have a length of 50 μm, and *dcap* is a variable parameter that symbolizes the air gap between the cantilever tip and the ring surface, which is the same as the anchor's thickness in simulations. Both thicknesses of the Au and Si layers are 0.5 μm.

The SRRs of the sensor can be excited by two distinct methods. In the first method, a plane wave is incident on the face of the SRRs as illustrated in Fig. 2. It should be noted that an incident electromagnetic (EM) wave must excite the magnetic resonance of the SRR through magnetic coupling in which the external magnetic field (H-field) should be polarized perpendicular to the SRR plane, i.e. the direction of propagation should be parallel to the SRR. However, if the direction of propagation is normal to the SRR plane and the incident electric field (E-field) is parallel to an imaginary line crossing the slits (Fig. 2), the E-field coupling can induce the magnetic resonance of the SRR [12]. In the second approach, a coplanar waveguide (CPW) is placed on the other side of the substrate, and the slits of the SRR, denoted by s, are aligned to a gap between the signal line and the ground plane, as illustrated in Fig. 3. Thus, the SRRs can be excited by the fringing field that travels along the CPW, which has an impedance of 50 Ω.

B. Radio Frequency Simulations

Since the electromagnetic (EM) fields of the cantilevers are mostly concentrated in the air region sandwiched between the cantilevers and the metal rings, the deflection of the micro-cantilevers is approximated with a uniform deflection across the whole length of the cantilevers in simulations and measurements. The relationship between the deflection of the cantilever tip and temperature is shown in Eq. (1) (see [11] for details), where δ denotes the deflection, α_1 and α_2 denote thermal expansion coefficients of the two layers, t_1 and t_2 denote the thicknesses of the two layers, and ΔT denotes the temperature change. From Eq. (1), the design of the cantilevers presented in Fig. 1 is estimated to have a sensitivity of 0.19 μm/°C.

$$\delta = \frac{\Delta T(\alpha_1 - \alpha_2)(1 + t_1/t_2)\mathrm{Lcant}^2}{2(t_1 + t_2)} \quad (1)$$

The simulation results of the first excitation approach, as presented in Fig. 2, are shown in Fig. 4. In this model, only one cantilever is implemented per SRR, which is positioned over the split of the inner rings. The two resonance modes observed

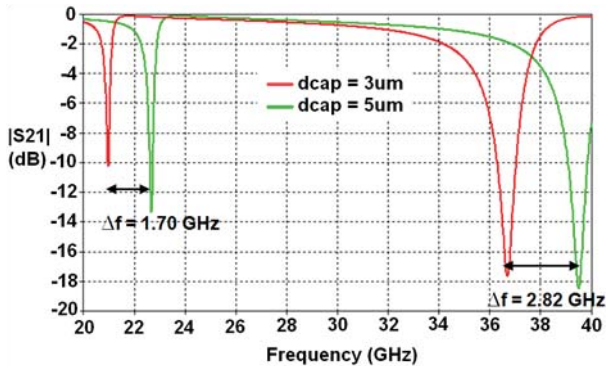

Fig. 4. Magnitude of transmission coefficient S_{21} of the sensor in the first excitation configuration shown in Fig. 2.

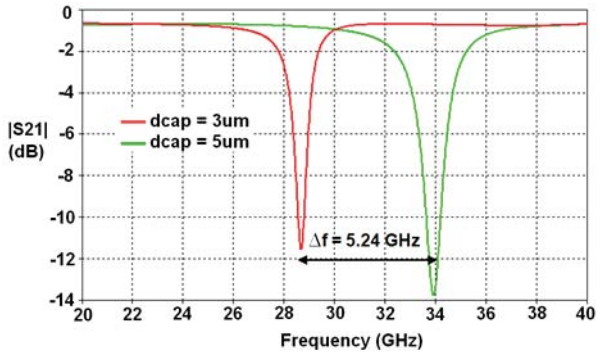

Fig. 5. Magnitude of transmission coefficient S_{21} of the sensor in the second excitation configuration shown in Fig. 3.

in this frequency range (between 20–40 GHz) are excited by the two rings in this structure. Observed from Fig. 4, the highest sensitivity is shown to be 1.41 GHz/μm, corresponding to 268 MHz/°C using Au-Si bimorph cantilevers.

The simulation results of the second excitation approach, as presented in Fig. 3, are shown in Fig. 5. In this model, two cantilevers are implemented per SRR, one is positioned over the inner ring split, and the other is placed over the outer ring split. The resonances in Fig. 4 are different from those observed in Fig. 3 because the effective impedance in this structure is different from that presented in Fig. 2. From Fig. 5, the sensitivity is recorded as 2.62 GHz/μm, corresponding to 498 MHz/°C, i.e. 1.6% frequency shift per °C, more than two order of magnitude higher than the sensitivity reported in [5] where a slot resonator operating between 19.3–19.5 GHz was introduced with bimorph micro-cantilevers yielding a sensitivity of about 580 kHz/°C or 0.003% frequency shift per °C. In the slot design in [5], the cantilevers deflect from 200 μm to a flat position, corresponding to a temperature range of 25–300 °C.

III. Principles of Operation

The temperature sensing mechanism of the transducer is based on two uncoupled principles: 1) deflections of bimorph cantilevers in response to temperature changes and 2) resonant frequency shifts in response to deflections of cantilevers. Since they are two independent physical phenomena, they can be optimized separately.

A. Mechanical Response – the Deflection of the Cantilevers in Response to Temperature Change

The deflection is caused by the difference in thermal expansion coefficients of the two materials that constitute the two different layers of the cantilevers. This mechanism is well-known and has been utilized widely in numerous applications [11], [13]. As temperature changes the length of each cantilever layer expands at different rates. Since the two layers are bonded together, the cantilevers are bent in order to accommodate the different rates of change in the length of their layers. The deflection can be estimated utilizing (1) presented in Section II. The bimorph cantilevers can realize various operating ranges depending on the material choices given that they provide the linear mechanical deflection within the temperature range of interest. Despite extended thermal cycling, the bimorph cantilevers are robust, and they reliably return to the same position at a given temperature as long as they are operated within the range limits for a particular material choice [11]. In the fabrication of bimorph micro-cantilevers, the tips of the cantilevers are usually deflected, referred to as initial deflection, which is due to the stress and strain during different MEMS processes. The initial deflection is in equilibrium at room temperature; then, it changes in response to temperature changes. As a result, this initial deflection determines the resonances of the sensor at room temperature, which can be controlled to an acceptable tolerance. The discussion of this tolerance limit is not within the scope of this paper.

B. Electromagnetic Response – Resonant Frequency Shifts in Response to the Deflections of the Cantilevers

The split ring structure was first proposed in [14] and has attracted growing interest since. Many variations of SRRs have been proposed to realize materials with negative values of magnetic permeability, also known as metamaterials. The metamaterials, based on SRRs, are highly frequency selective suggesting that the SRR elements have a very high quality factor ($Q > 600$) [15], [16]. When the SRRs are excited, an electromotive force is induced around the rings. However, due to the slits on each ring, displacement currents flow from one ring to another across the slot between them; thus, the SRRs effectively inherit a distributed capacitance. As a result, the field at the slit on each ring has high intensity, which suggests that for any modification of the capacitance of these slots, the currents on the rings can be influenced significantly. Therefore, such change in the currents may induce a significant shift in the resonant frequencies. In the design proposed in Fig. 1, the metal layer (gold) of the cantilever constitutes the lower layer of the bimorph cantilever, which is supported by a gold anchor that shorts the bimorph cantilever to one end of the split ring. The free end of the bimorph cantilever effectively forms a parallel plate capacitance with the other end of the split ring, making the split gap capacitance sensitive to the deflection of the bimorph cantilever. Note that the split gap

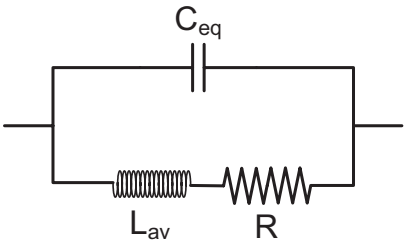

Fig. 6. RLC equivalent circuit of the temperature transducer.

capacitance also influences the distributed capacitance formed by the two concentric split rings.

To further understand how the frequency shift of the SRRs corresponds to the deflection of the cantilevers, an RLC equivalent circuit (Fig. 6) is employed to model the sensor. In Fig. 6, R accounts for the total losses at resonance, L_{av} is the average inductance comprising of the self-inductance of the inner and outer rings, and C_{eq} is the equivalent capacitance of the circuit comprising the capacitances at the two slits, C_{g1} and C_{g2}, and the total capacitance, C_t, distributed along the separation of the rings. Thus, the resonance can be approximated by Eq. (2) [17].

$$f = \frac{1}{2\pi(\mathrm{L_{av}C_{eq}})} \tag{2}$$

$$\mathrm{L_{av}} = (\mathrm{L_1} + \mathrm{L_2})/2 \tag{3}$$

$$\mathrm{C_{eq}} = \frac{\mathrm{Ct}}{4} + \mathrm{Cg_1} + \mathrm{Cg_2} \tag{4}$$

$$\mathrm{C_t} = 2\pi\,\mathrm{C_{pul}} \tag{5}$$

$$\mathrm{C_{gn}} \approx \frac{\in_o \mathrm{c_n t_n}}{\mathrm{s_n}} \text{ where n } = \begin{cases} 1 \text{ for inner ring} \\ 2 \text{ for outer ring} \end{cases} \tag{6}$$

The inductance in Eq. (3) is an approximation obtained from [17]. The mutual inductance between the two rings is neglected – only self-inductance of each ring remains in the equation. C_t s the total capacitance resulting from the separation of the two rings, which can be estimated by Eq. (5), in which r is the average radius of the two rings and C_{pul} is the distributed capacitance per unit length of two parallel strip lines [18], [19]. C_{g1} and C_{g2} represent the capacitances at the splits (not loaded with cantilevers) of the inner and outer rings respectively, and can be approximated as parallel plate capacitances shown in Eq. (6), in which c is the width of the ring strip, t is the metal thickness, and s is the split gap (Fig. 1). This model has been studied in literature and shown to be sufficiently accurate in modeling the resonant behavior of the conventional double split rings [16], [17], [19]. In most applications of SRRs, the split capacitances are relatively small and can be neglected. However, in the temperature sensor proposed here, where the splits are loaded with cantilevers, the values of the split capacitances, C_{g1} and C_{g2}, vary by about an order of magnitude over the operation range of the sensor, resulting in large shifts of the resonant frequencies as the displacement *dcap* changes due to the deflection of the bimorph cantilevers. This is because these capacitances can be estimated approximately as $\varepsilon_o c \Delta x$ / *dcap*, where c is the width of the ring strip and the cantilever, Δx is the overlap length of the cantilevers and the rings, and *dcap* is the height of the cantilevers with respect to the ring surface. Therefore, as *dcap* increases, C_{g1} and C_{g2} decrease; hence, the resonant frequencies increase according to Eq. (2) (Figs. 4 and 5). Observe that the rate of change of capacitance is proportional to *1/dcap*^{2} which would give higher sensitivity as *dcap* is decreased. On the other hand, if the cantilever gap *dcap* is decreased below certain limit, the circuit would appear as a short circuit to the operating frequency. Therefore, to give the sensor a good dynamic range for a given sensitivity, the initial gap should be chosen appropriately given the limitations of the fabrication technology. Furthermore, fully obtaining the resonant frequency as a function of the cantilever deflection is not trivial and is investigated in the next step of this work. Once the applications specify the temperature operating range, the choice of the materials, which is limited by the working environment, should be chosen to produce the largest difference between the thermal expansion coefficients of the two layers that constitute the bimorph cantilevers. Next, the desired sensing range (deflection induced by temperature change) should fit the linear range of the sensor's electromagnetic response due to its strong dependence on the choice of the initial deflection. Demonstration of such optimization is not within the scope of this paper.

IV. Fabrications and Measurements of Proof-of-Concept Prototypes

As stated in Section III, the operation of the first principle is independent from that of the second principle; hence, these two uncoupled mechanisms can be optimized separately. As a result, the sensitivity and the upper and lower limits of the temperature sensing range are determined mostly by the choice of materials utilized in the bimorph cantilevers. To demonstrate the proof-of-concept of the proposed temperature transducer, lower frequency prototypes were constructed around 3–5 GHz due to fabrication limitations. The size of the cantilevers was scaled up so they could be fabricated with quick and manual processes. Prototypes of both excitation methods (Figs. 2 and 3) were constructed. It should be noted that in the first prototype design (Fig. 2), only one cantilever is loaded, while two cantilevers are loaded on the second prototype design (Fig. 3).

A. Fabrications and Characterizations of Cantilevers

In the low frequency prototypes, the cantilevers were made from a 100 μm thick Al sheet. A smaller sheet of PET (Polyethylene terephthalate) with different thicknesses was laminated on top of the Al sheet. Then, the two sheets were diced, 1mm into the side of the Al-PET and 1.5 mm into the side of PET to form cantilevers with attached anchor, thus making 2.5 mm long cantilevers assembled with a PET anchor and preset thicknesses (Fig. 7). In this formation, PET was the anchor's material. The cantilevers were then stamped onto the SRR, over the splits, and mechanically stabilized with conductive epoxy at one end. The conductive epoxy also serves to short the cantilevers to the rings (Fig. 7). The air gaps between cantilevers and rings, denoted as *dcap* in

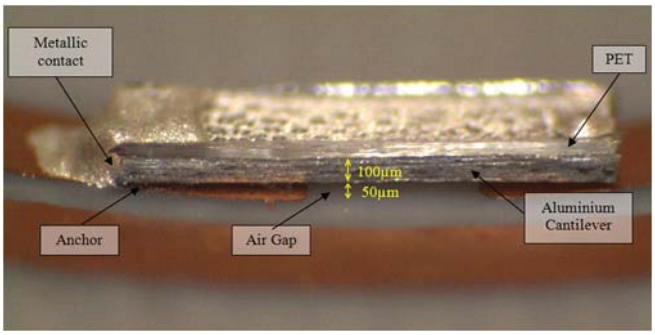

Fig. 7. Capture of an Al-PET bimorph cantilever under microscope with PET anchor of 50-μm thickness.

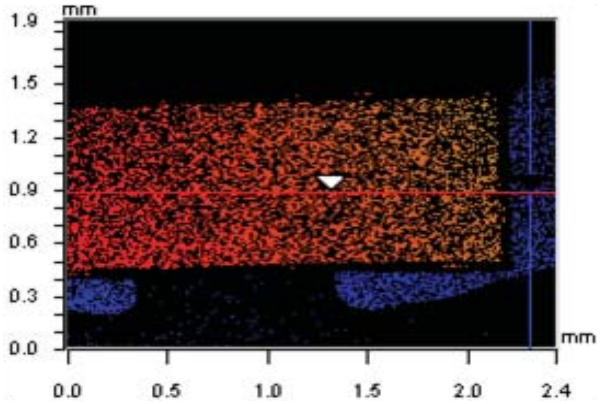

Fig. 8. Top view capture of a cantilever from optical scan.

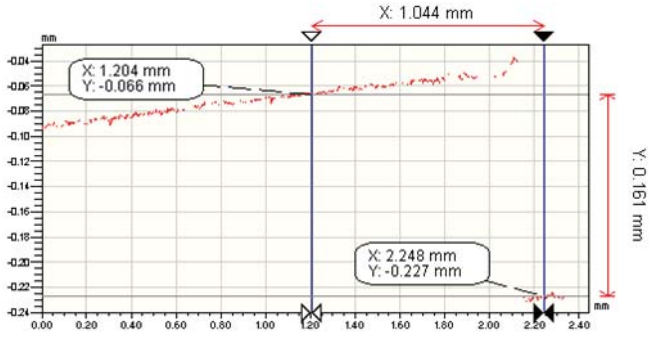

Fig. 9. Plots of optical surface scan along a line about the center of the cantilever and ring surface.

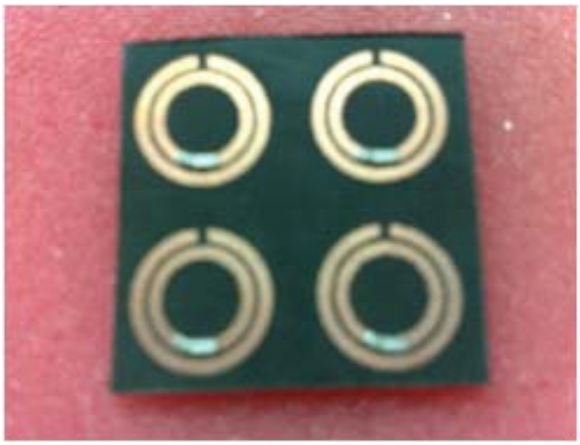

Fig. 10. Array of four SRRs loaded with bimorph cantilevers.

Fig. 1, were measured with an optical scanner (a profilometer) after the assembly. Two samples with different anchor heights were fabricated to emulate the uniform deflection of the cantilevers. When SRRs are loaded with these cantilevers, without inducing temperature change, the frequency measurements on these samples could validly demonstrate the second operation principle (the electromagnetic responses for a given deflection) of the sensor. Note that although this formation of the cantilevers for prototypes operating around 4–6 GHz range utilizes different materials from the cantilever formation shown in Fig. 1 (PET and aluminum instead of silver and silicon in the respective order), the split ring structures loaded with the bimorph cantilevers in Fig. 2 and 3 share the same circuit topology (Fig. 6) with those in Fig. 10, 13. Recall that the operation of the sensor is based on two independent principles (Sect. III), in which the mechanical principle (deflection versus temperature) is well-known. Thus, the proof-of-concept prototypes presented in the subsections IV B-C seek to validate the electromagnetic principles, from which the frequency shifts occur as observed in the thermally static RF simulations. The order of the bimorph cantilever layers would only affect the deflection direction of the cantilevers (up or down) for a given temperature change (increased or decreased) but not the range of the deflection. In all of the thermally static RF simulations presented in this work, the deflection direction of the cantilevers does not influence the frequency shifts but only the range of the deflection does. An optical measurement capture is shown in Fig. 8 where the surface height is coded in color. Different reflecting points along the red line in Fig. 8 are plotted in Fig. 9, where the cantilever in the measurement is shown to slightly deflect upwards after the assembly and annealing processes.

B. Fabrications and Measurements of the Temperature Sensor Prototype Built for Incident Wave Excitation

Four SRRs, each loaded with one cantilever, were fabricated into 2×2 array configuration as shown in Fig. 10 without a ground plane. The substrate was RT5870 ($\varepsilon_r = 2.33$, substrate thickness $= 787$ μm). The dimensions of the SRRs are as follows: $r_{int} = 3.5$ mm, $c = 1.0$ mm, $d = 0.5$ mm, and $s = 1.0$ mm.

The measurements were performed with a horn antenna and a vector network analyzer (VNA). Reflection-only calibration was performed using short, open, and load standards. To obtain temperature measurements, a horn antenna was directed at the sample as shown in the setup (Fig. 11). The sample was attached onto a foam mat, and the temperature probe was placed next to the sample. The horn antenna was connected to the VNA for a 1-port measurement, and S_{11} was recorded. At first, the temperature surrounding the sample was heated up to about 100 °C with a lamp. Since this was an open environment, it was difficult to obtain the steady state of temperature since the heated air was diffused quickly away from the heated sample. Therefore, the temperature was allowed to cool down

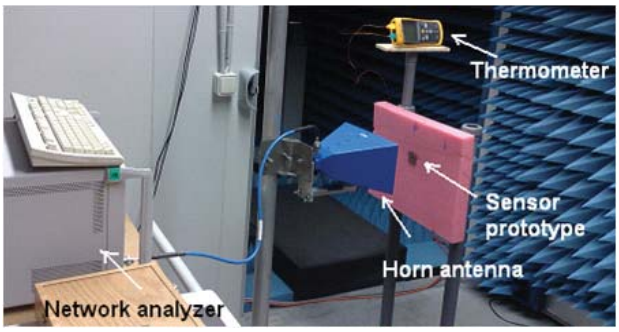

Fig. 11. Temperature measurement setup.

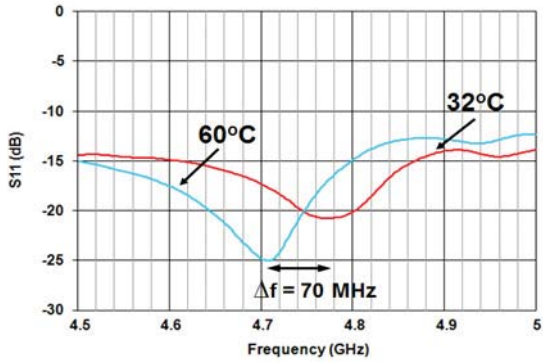

Fig. 12. Frequency response for two different temperatures of the prototype with a four-SRR array loaded with cantilevers.

until the reading on the thermometer became relatively stable. Also because of the open environment and limitations in the test conditions, an array of four ring sets was chosen in this test to achieve relatively uniform temperature induced by the lamp. Then, the temperature and S_{11} results could be recorded. With such a measurement setup, only two data sets corresponding to two temperature points of 60 °C and 32 °C could be validly recorded in which the temperature appeared to be relatively stable with a tolerance of about +/− 5 °C. However, in this demonstration only the difference in temperature is important. The plot of this measurement is shown in Fig. 12, which shows a resonant frequency shift of 70 MHz, from 4.77 GHz to 4.70 GHz, corresponding to a sensitivity of 2.5 MHz/°C, i.e. 0.05% of frequency shift per degree based on the center operating frequency of 4.735 GHz . In comparison to the sensitivity of 580 kHz/°C as reported in [5], i.e. 0.003% of frequency shift per degree based on center operating frequency of 19.36 GHz (Fig. 8 in [5]), our transducer prototype at 4.7 GHz is 17 times more sensitive. The sensitivity achieved for this prototype is not proportional to that reported in the millimeter-wave model in terms of dimension ratio because it is largely limited by the Al-PET bimorph cantilevers in the mechanical responses to temperature changes as opposed to the Au-Si material choice. In this setup, the height of the cantilevers cannot be recorded during measurements so the sensitivity (frequency shift per deflection unit) is not reported. Due to limitations of fabrication and measurements, the linearity response of the sensor is not addressed in this prototype. In order to investigate the linearity response of the sensor design, a better controlled environment for temperature measurements was constructed for the prototype excited with the CPW.

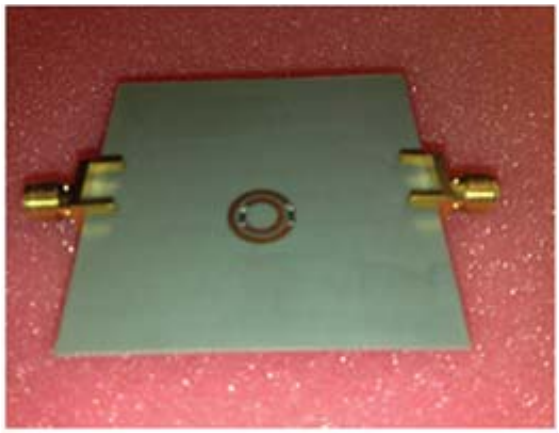

Fig. 13. Sensor prototype with CPW excitation.

C. Fabrications and Measurements of the Temperature Sensor Prototype Built for CPW Excitation

In this configuration, the SRRs are loaded with two bimorph cantilevers and are excited by the traveling field of the CPW printed on the other side of the substrate (Fig. 13). The prototype was realized on Neltec N9217 substrate (ε_r = 2.17, substrate thickness = 787 μm). The dimensions of the SRRs in this model are as follows: r_{int} = 2.5 mm, c = 1.0 mm, d = 0.5 mm, and s = 1.0 mm. The width of the signal line is 4 mm (50 Ω of impedance), and the ground-signal separation is 150 μm. Since there is little control over this process of fabrication (discussed in Section IV-A, the cantilevers assembled on the same prototype have different heights. Two prototypes were built, and the average heights of the cantilevers are approximately 128 μm and 101 μm for each pair of the cantilevers assembled on the two prototypes.

1) Frequency response measurements at room temperature for prototypes with different cantilever heights for uniform deflection approximation.

The simulated and measured results for this design are shown in Fig. 14. It should be noted that after the optical characterization step to evaluate the heights of the cantilevers was performed, the measured height values were used in simulations; therefore, the simulated models corresponded to the physical prototypes. Note that the simulations presented in Fig. 14 have the same configuration, materials, and dimensions of the prototype shown in Fig. 13. The simulations were performed with the actual *dcap* values obtained from the profilometer measurements (Fig. 9) of the sensor prototype in order to validate the theoretical prediction of the frequency shifts. The plots in Fig. 14 show good correlation between simulations and measurements in terms of resonant frequency peaks. Thus, the agreement in Fig. 14 directly validates the electromagnetic principles behind the frequency shifts corresponding to fixed *dcap* values representing a given deflection of the cantilevers. Consequently, the results also indirectly validate the electromagnetic responses observed in the thermally

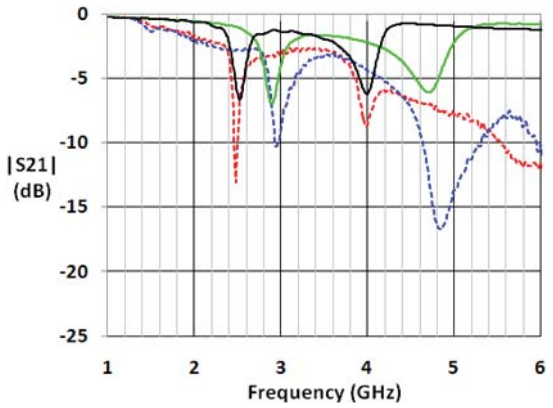

Fig. 14. Magnitude of S_{21} for the SRR sensor prototype with solid black curve is simulated results of $dcap = 101\ \mu$m model, solid green curve is simulated results of $dcap = 128\ \mu$m model, dashed red curve is measured results of $dcap = 101\ \mu$m sample, dashed blue curve is measured results of $dcap = 128\ \mu$m sample.

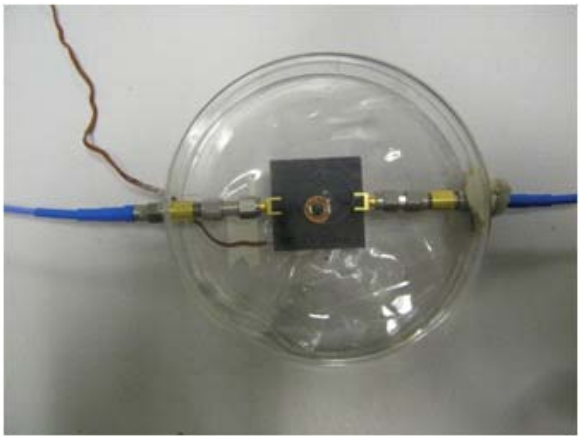

Fig. 15. Close environment construction of the CPW prototype for direct temperature measurement.

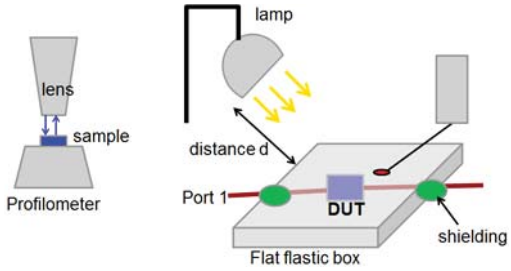

Fig. 16. Temperature measurement setup.

static RF simulations shown in Figs. 4 and 5 because of the same circuit topology that the two structures share. On the other hand, electromagnetic behavior of the sensor responses to real time dynamic temperature changes (including the mechanical response of deflection versus temperature change) is presented in Fig. 12 and Fig. 18 (next subsection). In Fig. 14, the low value of S_{21} in the measurements reflects a high insertion loss due to the transition between CPW and the coaxial cable. Unfortunately, due to limitation of fabrication and assembly of this transition specifically to this prototype, the control of the fabricated dimensions was less than perfect. There were gaps between the SMA connectors and the CPW signal line, and the SMA outer radius was also slightly smaller than the width of the CPW signal line that caused reflection as the signal was launched into the CPW. However the negative effect has little significance concerning the proof-of-concept. A frequency shift of about 800 MHz, from 4 GHz of the 101 μm *dcap* sample to about 4.8 GHz of the 128 μm *dcap* sample, is observed resulting in a sensitivity of about 30 MHz/μm that is approximately two orders of magnitude higher than the 700 kHz/μm reported in [5], which is based on a 19 GHz resonating slot. Note that this comparison is in terms of how well the resonator is designed to convert a cantilever deflection into a frequency shift, whereas the conversion of temperature change into cantilever deflection is an independent principle.

2) Frequency response measurements with respect to different temperatures.

In this measurement, a close environment surrounding the transducer prototype was constructed. The prototype was concealed in a small plastic box having two coaxial cables connected to the device through the sides of the box as shown in Fig. 15. The open holes, where the cables access the device, were sealed with rubber to ensure a closure. The temperature probe was inserted next to the sample and also running through the side of the box to connect to an external thermometer for temperature monitoring. The sample and the air trapped inside the box were then heated to 100 °C with a lamp and then allowed to cool down. It should be noted that the lamp was kept at a constant distance d from the sample to maintain constant illumination of thermal flux as illustrated in Fig. 16. Thus, at any given temperature, distance d could be adjusted so the temperature inside the box could be brought into thermal equilibrium with the outside region illuminated by the lamp. This configuration also allowed for the characterization of the height of the cantilevers loaded on the rings without removing the prototype from the box. The captured image, shown in Fig. 17, presents the actual setup with VNA and SMA connectors present. The lamp was removed after heating to avoid interference with the RF reading during the cool-down process. The temperature readings from the probe decreased at a much slower rate because heat diffusion was taking place instead of air diffusion. As a result, the temperature reading was obtained in the range of 54 °C to 20 °C with a significantly improved tolerance of about +/− 1 °C. It should also be noted that it took about 10–15 minutes for each temperature step in this measurement and about an hour and a half for temperature to be heated up to 100 °C and then cooled down to about 27 °C. The sample was allowed to cool overnight, and the measurement at room temperature (recorded to be 20 °C) was carried out on the following day. The measurement results are shown in Fig. 18, where six different temperature responses were recorded. The plots show a relatively linear response of frequency shifts from 4.85 GHz at 47 °C to about 4.80 GHz at 20 °C, a sensitivity of 1.85 MHz/°C or a 0.04% frequency shift per °C. This sensitivity is slightly lower but on the same order of magnitude

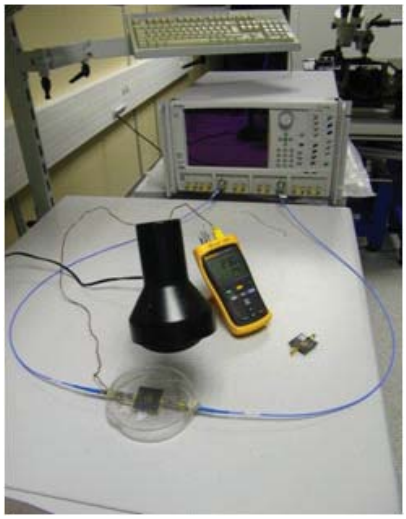

Fig. 17. Image of temperature measurement setup with VNA (blue cables) and with the reference temperature probe inserted inside the plastic box (brown wire).

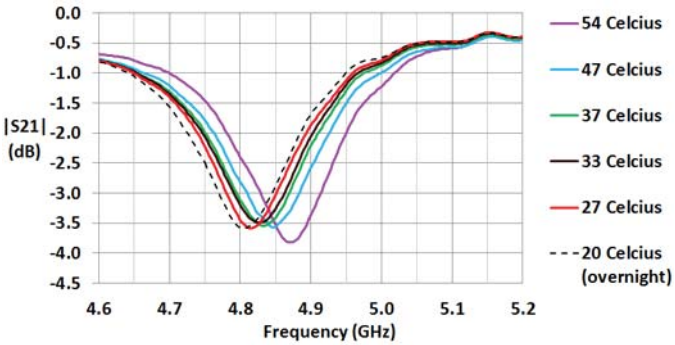

Fig. 18. Frequency response of the temperature sensor prototype excited with CPW at different temperatures.

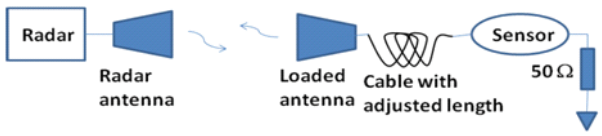

Fig. 19. RCS measurement system for remote sensing and identification.

with 0.05% of frequency shift per °C reported in Section IV-B, which was obtained with higher tolerance in the measurements. The curve of 54 °C appears to be nonlinear indicating the limit of the linear region of operation. In a practical implementation, the linear region of each operational principle should be characterized to obtain the overall linear response for the temperature transducer in terms of frequency shift versus temperature change. It is worth noting that in previous measurements of Section IV-B, one temperature point at 62 °C is outside of the linear range of response as indicated in Fig. 18, which explains the higher recorded sensitivity of the sensor prototype in Fig. 10.

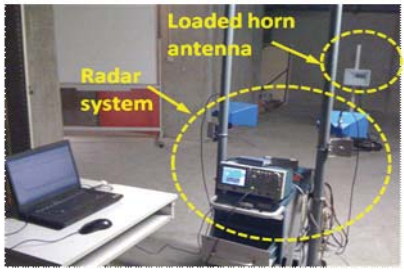

Fig. 20. Captured image of RCS measurement system.

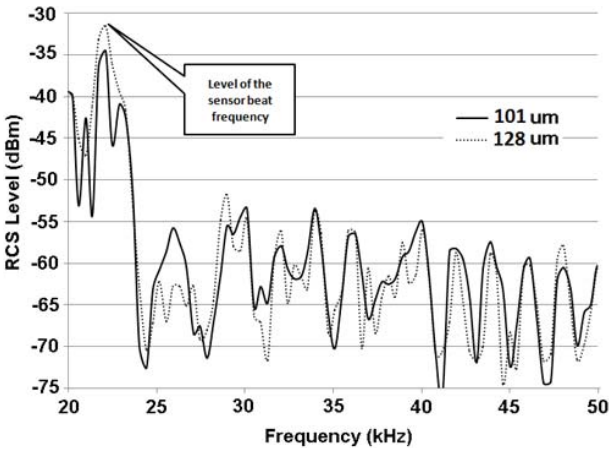

Fig. 21. RCS measurements of the low frequency prototypes for one sensor sample with *dcap* of 101 m (solid line) and another sample with *dcap* of 128 m (dashed line).

V. RCS Measurements and Remote Sensing Implementation of the Temperature Transducer

A frequency modulated continuous wave (FMCW) radar operating at 3 GHz was utilized as an interrogation device in the communication system illustrated in Fig. 19. In this technique of remote identification and data acquisition, the radar transmits RF signals and receives a modified response from the sensors while signals scattered from the rest of the environment remain unmodified. The loaded horn antenna, located 3.5 m away from the terminal of radar system, operates in the band of 1.8 GHz to 3.4 GHz with a gain of 15 dBi. The sensor prototype is treated as a load on the horn antenna side of the system and is terminated with a 50 Ω load at the end of a 13 m long cable. The captured image of the radar cross-section (RCS) measurement system is shown in Fig. 20. Based on the total travel distance of the signals, each object gives a different beat frequency with a different RCS level. Although multipath reflections are possible, the signal level is negligibly low (close to noise level). The corresponding beat frequency for the sensor prototype (Fig. 13) in this setup is 22 kHz as indicated in Fig. 21. At this frequency, the fluctuation of the RCS level between the two average *dcap* values (101 μm and 128 μm) of the two prototypes is observed to be about 3 dBm. Thus, with different lengths of the transmission lines connecting the sensor nodes with the communicating antenna, i.e. the loaded horn antenna in this setup (Fig. 19), the positions of different sensor nodes in this passive sensing

network can be identified (indicated by beat frequencies) along with its sensing information (indicated by RCS levels). When the measurements were repeated twice (with one day in between each measurement), the same RCS fluctuation was observed. Thus, the RCS readings corresponding to the two *dcap* values are shown to be capable of reliable sensing. Note that in this example of implementation, the horn antenna is conveniently used as the communication antenna (the loaded antenna in Fig. 19). In practice, it could be replaced by low profile highly directive antenna arrays, such as a highly compact Yagi-type array of patch antennas [20], [21].

VI. Conclusion

A new wireless passive ultrasensitive temperature transducer based on SRRs and bimorph cantilevers is developed establishing a new class of RF sensors. The transducer can potentially operate up to the millimeter-wave frequencies around 30 GHz based on two principles: well-known cantilever deflections induced by temperature changes, and the newly introduced principle of SRR resonant frequency shifts induced by the deflection, of cantilevers. The newly designed sensor is shown in simulations to have a high sensitivity of frequency shift to cantilever deflection (2.62 GHz/μm), corresponding to 498 MHz/°C or 1.6% of frequency shift per °C for the operating frequency around 30 GHz. The presented transducer design is completely passive, miniaturized, and has a high quality factor that allows high resolution of sensing which may enable integration of different types of sensors without saturating the operating frequency band of the sensing system, thus achieving multiphysics sensing in a single passive network. Scaled prototypes were also designed, fabricated, and presented in this paper to illustrate the proof-of-concept of the sensor. The scaled models operated around 4 GHz, and measurements were performed with a heat source that resulted in a sensitivity of 2.5 MHz/°C and 1.82 MHz/°C or 0.05% and 0.04% of frequency shift per °C, respectively for the two sensor designs featuring 1-2 orders of magnitude in improvement over similar wireless sensors. In addition, the RCS measurements of the temperature sensor prototype, implemented in the newly proposed technique of remote sensing and identification, demonstrate a correlation between the deflection of the cantilevers of the sensor and the observable RCS at a particular beat frequency. As a result, this system is capable of remote sensing and identification that could potentially enable "rugged" and completely passive sensor networks. Such sensor networks can be implemented, for example, on the wings of aircraft while the temperature can be read remotely and continuously in real time from the cabin of the aircraft with a radar system. This type of sensor is currently characterized by lower resolution in temperature detection compared to those in CMOS technology but offer tremendous advantages of being passive and wireless.

Acknowledgment

The authors would like to thank T. Idda and S. Bouaziz, CNRS-LAAS, Toulouse, France, for their assistance in measurements.

References

[1] P. R. N. Childs, J. R. Greenwood, and C. A. Long, "Review of temperature measurement," *Rev. Sci. Instrum.*, vol. 71, no. 8, pp. 2959–2978, Aug. 2000.

[2] J. Goetz, "Sensors that can take the heat–Part 1," *Sensors*, vol. 17, no. 6, pp. 20–38, Jun. 2000.

[3] O. J. Gregory and T. You, "Ceramic temperature sensors for harsh environments," *IEEE Sensors J.*, vol. 5, no. 5, pp. 833–838, Oct. 2005.

[4] L. Toygur, "Interface circuits in SOI-CMOS for high-temperature wireless micro sensors," Ph.D. dissertation, Dept. Electr. Electron. Eng., Case Western Reserve Univ., Cleveland, OH, Jan. 2004.

[5] S. Scott and D. Peroulis, "A capacitively-loaded MEMS slot element for wireless temperature sensing of up to 300 °C," in *Proc. IEEE Int. Microw. Symp.*, Boston, MA, Jun. 2009, pp. 1161–1164.

[6] M. M. Jatlaoui, P. Pons, and H. Aubert, "Pressure micro-sensor based on radio-frequency transducer," in *Proc. IEEE Int. Microw. Symp.*, Atlanta, GA, Jun. 2008, pp. 15–20.

[7] T. T. Thai, G. R. DeJean, and M. M. Tentzeris, "A novel front-end radio frequency pressure transducer based on a millimeter-wave dual-band resonator for wireless sensing," in *Proc. IEEE Int. Microw. Symp.*, Boston, MA, Jun. 2009, pp. 1701–1704.

[8] M. M. Jatlaoui, F. Chebila, P. Pons, and H. Aubert, "New micro-sensors identification techniques based on reconfigurable multi-band scatterers," in *Proc. Asia-Pacific Microw. Conf.*, Singapore, Dec. 2009, pp. 968–971.

[9] M. M. Jatlaoui, F. Chebila, P. Pons, and H. Aubert, "Wireless interrogation techniques for a passive pressure micro-sensor using an EM transducer," in *Proc. Eur. Microw. Conf.*, Rome, Italy, Sep.–Oct. 2009, pp. 53–56.

[10] T. T. Thai, F. Chebila, J. M. Mehdi, P. Pons, H. Aubert, G. R. DeJean, M. M. Tentzeris, and R. Plana, "A novel passive ultrasensitive RF temperature transducer for remote sensing and identification utilizing radar cross sections variability," in *Proc. IEEE APSURSI*, Toronto, ON, Canada, Jul. 2010, pp. 1–4.

[11] R. J. Stephenson, A. M. Moulin, and M. E. Welland, "Bimaterials thermometers," in *The Measurement Instrumentation and Sensors Handbook*. Boca Raton, FL: Chemical Rubber, 1999.

[12] N. Katsarakis, T. Koschny, M. Kafesaki, E. N. Economou, and C. M. Soukoulis, "Electric coupling to the magnetic resonance of split ring resonators," *Appl. Phys. Lett.*, vol. 84, no. 15, pp. 2943–2945, 2004.

[13] C.-Y. Lee, C.-H. Tsai, L.-W. Chen, L.-M. Fu, and Y.-C. Chen, "Elastic-plastic modeling of heat-treated bimorph micro-cantilevers," *Microsyst. Technol.*, vol. 12, nos. 10–11, pp. 979–986, Aug. 2006.

[14] J. B. Pendry, A. J. Holden, D. J. Ribbins, and W. J. Stewart, "Magnetism from conductors and enhanced nonlinear phenomena," *IEEE Trans. Microw. Theory Tech.*, vol. 47, no. 11, pp. 2075–2084, Nov. 1999.

[15] D. Smith, W. J. Padilla, D. C. Vier, S. C. Nemat-Nasser, and S. Schultz, "Composite medium with simultaneously negative permeability and permittivity," *Phys. Rev. Lett.*, vol. 84, no. 18, pp. 4184–4187, May 2000.

[16] R. Marques, F. Mesa, J. Martel, and F. Medina, "Comparative analysis of edge- and broadside-coupled split ring resonators for metamaterial design - theory and experiments," *IEEE Trans. Antennas Propagat.*, vol. 51, no. 10, pp. 2572–2581, Oct. 2003.

[17] M. Shamonin, E. Shamonina, V. Kalinin, and L. Solymar, "Resonant frequencies of a split-ring resonator: Analytical solutions and numerical simulations," *Microw. Opt. Technol. Lett.*, vol. 44, no. 2, pp. 133–136, Jan. 2005.

[18] P. Hammond and J. Sykulski, *Engineering Electromagnetism: Physical Processes and Computation*. Oxford, U.K.: Oxford Univ. Press, 1994.

[19] R. Marqués, F. Mesa, J. Martel, and F. Medina, "Comparative analysis of edge- and broadside-coupled split ring resonators for metamaterial design - theory and experiments," *IEEE Trans. Antenas Propagat.*, vol. 51, no. 10, pp. 2572–2581, Oct. 2003.

[20] T. T. Thai, G. R. DeJean, and M. M. Tentzeris, "Design and development of a novel compact soft-surface structure for the front-to-back ratio improvement and size reduction of a microstrip Yagi array antenna," in *Proc. IEEE Antennas Propagat. Soc. Int. Symp.*, Honolulu, HI, Jun. 2007, pp. 1193–1196.

[21] G. R. DeJean, T. T. Thai, S. Nikolaou, and M. M. Tentzeris, "Design and analysis of microstrip Bi-Yagi and quad-Yagi antenna arrays for WLAN applications," *IEEE Antennas Wireless Propagat. Lett.*, vol. 6, pp. 244–248, Apr. 2007.

Trang T. Thai received the B.Sc. degree in electrical engineering and the B.Sc. degree in physics from the Georgia Institute of Technology, Atlanta, in May 2008, where she is currently pursuing the Ph.D. degree in electrical engineering. Her Ph.D. thesis is advised by Prof. Manos Tentzeris and co-advisor Dr. Gerald DeJean.

She was invited to perform research at the French National Scientific Research Center-Laboratory of Analysis and Architecture of Systems (LAAS), Toulouse, France, under the supervision of H. Aubert from 2009 to 2010 for approximately a year. The collaboration with LAAS has continued into present days. She was with Microsoft Research, Redmond, WA, as a Research Intern from 2010 to 2013. Her research at Microsoft has been centered around proximity sensing for gesture recognition, on-body communication channels, and other wearable sensing platforms in order to enable new dimensions of human-machine interactions and new capabilities in non-invasive sensing of body physiological parameters. Her Ph.D. thesis work includes designs and developments of radio frequency (RF) transducers for pressure, temperature, and strain sensing, all of which pioneer a new class of transducers that are based on RF principles. Other work includes sensing based on nanomaterials, such as carbon nanotubes as well as material characterization, front-end devices in microwave engineering, and surface plasmon RF sensing applications. Her current research interests include RF sensing with multidisciplinary approach.

Ms. Thai was a recipient of the Microsoft Research Ph.D. Fellowship in 2011.

Jatlaoui M. Mehdi received the Diploma degree in telecommunications engineering from the National Engineering School of TUNIS, Tunisia, in 2004, and the M.S and Ph.D. degrees in microwaves, electromagnetism, and optoelectronics from the National Polytechnic Institute of Toulouse, Toulouse, France, in September 2005 and April 2009, respectively.

He is currently a Research Engineer with the French National Scientific Research Center—Laboratory of Analysis and Architecture of Systems (CNRS-LAAS), Toulouse. He is interested in developing wireless passive microsytems based on the electromagnetic transduction principle for passive remote sensing. During his Doctoral studies, he acquired a theoretical and practical background dealing with such microsystems development (theory, electromagnetic modeling, RF design, EM simulations, fabrication processes in the CNRS-LAAS cleanroom, and on-wafer antenna/RF/pressure measurements). His current research interests include wireless interrogation techniques based on FMCW radar, integrated packaging for RF and wireless applications using organic flexible substrates, passive sensors, microwave microelectromechanical systems, systems-on-package, 3-D heterogeneous integration of communicating nano-objects, integrated (multiband, conformal) antennas, and flexible electronics.

Franck Chebila received the Ph.D. degree in electronics engineering from the National Polytechnic Institute of Toulouse, Toulouse, France, in 2011.

He has 12 years of experience as a Microwave Circuit Design Engineer in the aerospace engineering sector. He joined the French National Scientific Research Center—Laboratory of Analysis and Architecture of Systems, Toulouse, in 2007, where he is currently a Research Engineer. His current research interests include radar interrogation techniques for passive sensors and wireless sensor networks.

Hervé Aubert (SM'99) was born in Toulouse, France, in July 1966. He received the Eng.Dipl. degree in July 1989 and the Ph.D. degree (High Hons.) in January 1993 from the Institut National Polytechnique (INPT), Toulouse, both in electrical engineering.

He has been a Professor at INPT since February 2001. He joined the French National Scientific Research Center—Laboratory of Analysis and Architecture of Systems, Toulouse, in February 2006. From April 1997 to March 1998, he was a Visiting Associate Professor with the School of Engineering and Applied Science, University of Pennsylvania, Philadelphia. He was the Co-Chairman of the Electronics Laboratory, INPT, from July 2001 to January 2005, and the Head of the Electromagnetics Research Group from July 2002 to September 2005. From September 2004 to September 2011, he was the Director of the Research Master Program in Microwaves, Electromagnetism and Optoelectronics, Toulouse. He has performed research work on integral-equation and variational methods applied to electromagnetic wave propagation and scattering. He has authored or co-authored one book, two book chapters, and 61 papers in refereed journals, and over 165 communications in international symposium proceedings. He holds five international patents in the area of antennas. His current research interests include the electromagnetic modelling of complex (multi-scale) structures. He has contributed to the books, *Fractals: Theory and Applications in Engineering* (Springer, 1999), *Micromachined Microwave Devices and Circuits* (Romanian Academy Edition, 2002), and the *New Trends and Concepts in Microwave Theory and Techniques* (Research Signpost, 2003).

Dr. Aubert is the Secretary of the IEEE Antennas and Propagation French Chapter and was the Vice-Chairman from 2004 to 2009. He is a member of the URSI Commission B.

Patrick Pons received the Ph.D. degree in electronics from Toulouse University, Toulouse, France, in 1990.

He has been a Researcher with the French National Scientific Research Center—Laboratory of Analysis and Architecture of Systems, Toulouse, since 1991. In 1995, he started a study on microtechnology for microwave applications. Currently, he manages the development of this technology for high frequency microsystems and also develops pressure sensors for specific applications. In 2005, he started research in a new field, coupling sensors and RF for the development of passive wireless sensors. His current research interests include microtechnology and microsensors.

Gerald R. DeJean received the B.S. degree in electrical and computer engineering from Michigan State University, East Lansing, in 2000, and the M.S. and Ph.D. degrees in electrical and computer engineering from the Georgia Institute of Technology (Georgia Tech), Altanta, in 2005 and 2007, respectively.

He is currently with Microsoft Research, Redmond, WA, as a Researcher in RF and antenna design. In November 2008, he was an Adjunct Assistant Professor with Georgia Tech. He has authored or co-authored over 50 papers in refereed journals and conference proceedings. He is interested in equivalent circuit modeling techniques to assist in the design and optimization of compact wireless devices. He is conducting research in remote sensing technologies in the form of pressure, temperature, user proximity. Currently, he is working on the implementation of on-body communications for health monitoring and ubiquitously secure data. He has dedicated his research to making the antenna more compact and integrable with multilayer packages, such as low temperature cofired ceramic, liquid crystal polymer, and multilayer organic, while maintaining the full functionality of the device for wideband and/or multiband applications. His current research interests include antenna design, RF and microwave design and characterization, and 3-D systems-on-package integration of embedded functions that focuses largely on modern commercial RF systems, such as cellular phones for PCS applications, Bluetooth and 2.4 GHz ISM applications, RFIDs, WLAN (802.11a,b,g), LMDS, and millimeter-wave applications at 60 GHz.

Manos M. Tentzeris (S'89–M'92–SM'03–F'10) was born in Piraeus, Greece. He received the Diploma degree in electrical engineering and computer science (*magna cum laude*) from the National Technical University, Athens, Greece, in 1992, and the M.S. and Ph.D. degrees in electrical engineering and computer science from the University of Michigan, Ann Arbor, in 1993 and 1998, respectively.

He is currently a Professor with the School of Electrical and Computer Engineering (ECE), Georgia Institute of Technology, Atlanta. He is currently the Head of the Electromagnetics Technical Interest Group, School of ECE. He has published more than 420 papers in refereed journals and conference proceedings, four books, and 19 book chapters. He has served as the Georgia Electronic Design Center Associate Director for RFID/Sensors Research from 2006 to 2010 and as the GT-Packaging Research Center (NSF-ERC) Associate Director for RF research and the Leader of the RF/Wireless Packaging Alliance from 2003 to 2006. He is the Head of the A.T.H.E.N.A. Research Group (20 students and researchers) and has established academic programs in highly integrated and multilayer packaging for RF and wireless applications using ceramic and organic flexible materials, paper-based RFIDs and sensors, inkjet-printed electronics, nanostructures for RF, wireless sensors, power scavenging and wireless power transfer, microwave MEMs, SOP-integrated (UWB, mutliband, conformal) antennas and adaptive numerical electromagnetics (FDTD, MultiResolution Algorithms).

Dr. Tentzeris was the Technical Program Co-Chair of the 54th ARFTG Conference in 1999, and he is currently a member of the Technical Program Committees of the IEEE-IMS, IEEE-AP, and the IEEE-ECTC Symposia. He was the TPC Chair for the IMS Conference in 2008 and the Co-Chair of the ACES Symposium in 2009. He was the Chairman for the IEEE CEM-TD Workshop in 2005. He was the Chair of the IEEE-CPMT TC16 in RF Subcommittee and he was the Chair of the IEEE MTT/AP Atlanta Sections for 2003. He is a member of the MTT-15 Committee, an Associate Member of the European Microwave Association, a fellow of the Electromagnetics Academy, and a member of the Commission D, URSI, and of the Technical Chamber of Greece. He is the Founder and Chair of the newly formed IEEE MTT-S TC-24 (RFID Technologies). He was an IEEE MTT-Distinguished Microwave Lecturer from 2010 to 2012.

Robert Plana was born in Toulouse, France, in March 1964. He received the Ph.D. degree from the French National Scientific Research Center—Laboratory of Analysis and Architecture of Systems (CNRS-LAAS), Toulouse, and Paul Sabatier University, Toulouse, in 1993.

He was an Associate Professor at CNRS-LAAS in 1993 and began new research concerning the investigation of millimeter-wave capabilities of silicon-based technologies. More precisely, he has focused on the microwave and millimeterwave properties of SiGe devices and their capabilities for low-noise circuits. In 1995, he started a new project concerning the improvement of the passives on silicon through the use of MEMS technologies. In 1999, he was with SiGe Semiconductor Inc., Ottawa, ON, Canada, where he worked on low-power and low-noise integrated circuits (ICs) for RF applications. In 2000, he was a Professor with Paul Sabatier University and Institut Universitaire de France, Paris, France. He has started a research team at CNRS-LAAS in the field of micro- and nanosystems for RF and millimeter-wave communications. Its main interests are technology, design, modeling, test, characterization, and reliability of RFMEMS for low-noise and high-power millimeter-wave applications and the development of the MEMS IC concept for smart microsystems. He has built a network of excellence in Europe in this field, AMICOM, regrouping 25 research groups. In 2004, he was appointed as a Deputy Director with the Department of Information and Communication, CNRS Headquarter, and from January 2005 to January 2006, as a Director. Since 2006, he has been the Head of a Research Group, CNRS-LAAS in the field of micro- and nanosystems for wireless communications. From November 2007 to November 2009, he joined the French Research Agency, Paris, where he is the Project Officer with the National Nanotechnology Initiative. Since November 2009, he has been the Head with the Department of Physic, Mathematics, Nanosciences and Nanotechnology, Information and Communication Technology, Ministry of Higher Education and Research, Paris, and is in charge of defining the French strategy for research and innovation. He is the author or co-author of more than 300 international journal and conference publications.

Dr. Plana was a recipient of the Special Award from CNRS for his works on silicon-based technologies for millimeter-wave communications.